Applied Physics Express **9**, 065801 (2016)
http://doi.org/10.7567/APEX.9.065801

Anisotropic charge carrier transport in free-standing hexagonal boron nitride thin films

Rajendra Dahal[1]*, Kawser Ahmed[1], Jia Woei Wu[1], Adam Weltz[2], James Jian-Qiang Lu[1], Yaron Danon[2], and Ishwara B. Bhat[1]*

[1]*Department of Electrical, Computer, and Systems Engineering, Rensselaer Polytechnic Institute, Troy, NY 12180, U.S.A.*
[2]*Department of Mechanical, Aerospace and Nuclear Engineering, Rensselaer Polytechnic Institute, Troy, NY 12180, U.S.A.*

*E-mail: dahalr.rpi@gmail.com; bhati@rpi.edu

Received March 12, 2016; accepted April 20, 2016; published online May 12, 2016

The in-plane and out-of-plane mobility–lifetime products of electrons and holes in free-standing hexagonal boron nitride (hBN) films are extracted from current–voltage characteristics of metal–hBN–metal structures measured under external excitations. The in-plane mobility–lifetime products for electrons and holes are ~2.8 x 10^{-5} and ~4.85 x 10^{-6} cm^2/V, measured from lateral carrier collection, whereas the out-of-plane mobility–lifetime products for electrons and holes are ~5.8 x 10^{-8} and ~6.1 x 10^{-9} cm^2/V, measured from vertical carrier collection, respectively. The mobility–lifetime product is a few orders of magnitude higher along the plane than along the out of plane in hBN films.
© 2016 The Japan Society of Applied Physics

Hexagonal boron nitride (hBN) is a layered material with unique features of ultrawide bandgap (~6 eV), high in-plane thermal conductivity, low density, high temperature resistance under extreme conditions, low dielectric constant, chemical inertness, and negative electron affinity.[1–3] These properties make hBN an ideal candidate for deep-UV optoelectronic devices (e.g., DUV light emitters, detectors, and electron emitters in field emission).[4,5] Furthermore, as structural analogs of graphene, two-dimensional hBN can serve as an excellent gate dielectric as well as substrate for graphene devices. The atomically flat hBN layer provides a smooth and flat interface without dangling bonds, which is a highly desired characteristic for high-carrier-mobility devices.[5,6] In addition to a broad spectrum of technical applications, hBN provides a unique opportunity to study the fundamental transport and optical properties of two-dimensional (2D) materials in three-dimensional (3D) form.[7] One of the applications of boron nitride is in the fabrication of high-efficiency solid-state thermal neutron detectors because ^{10}B has a reasonably good neutron absorption cross section (i.e., 3840 barn at 0.025 meV). The concept of the hBN detector is similar to that of the boron carbide detector, where the converter (boron) is part of the semiconductor material. In contrast to the boron-filled microstructured silicon neutron detector,[8] the hBN-based detector is homogeneous, in which the neutron-sensitive material and the charge collection region are the same.[9,10] In such a case, when a neutron interacts with a sufficiently thick hBN, charged particles are produced and lose their energy in the hBN material, where these charges can be collected to form a pulse. Thus, in an ideal case for every neutron interaction, there is a full charge collection, and the measured pulse height will be characterized by the Q value of the reaction (i.e., amount of energy released by the reaction, which is approximately 2.31 MeV for the B-10 dominant reaction). Charge trapping and edge effects can cause some reduction in this value; however, the neutron detection response could be fundamentally different from the response of the heterogeneous detector. The implication of this response is that a higher threshold can be set to cut the gammas from the spectrum without the loss of neutron detection efficiency, and thus such devices are expected to tolerate a much higher gamma background even when pulse pileup occurs. The response is similar to those of conventional BF_3 and He-3 detectors, without the bulkiness and the requirement of high voltage. Because of their ultrawide bandgap, hBN-based neutron detectors are expected to possess extremely low leakage current, enabling the fabrication of large-area detectors with a low gamma sensitivity and fast response. Furthermore, hBN-based neutron detectors could be operated at room temperature without any cooling hardware, which is superior to other small-bandgap semiconductor-based detectors, in which leakage current due to the recombination of thermally induced electron–hole pairs is an issue for large-area devices. Another advantage of hBN-based detectors is that they are less prone to radiation damage because of the structure of boron nitride, which enhances the reliability of the devices.

There has been significant progress in growing and fabricating heterojunction devices in hBN in recent years and hence there is an opportunity in exploiting this material for neutron detectors. Currently, there are two major issues with the hBN-based neutron detector: the growth of thick films and the charge collection from the highly anisotropic hBN layer. These limitations resulted in the low efficiency of current hBN detectors. In order to utilize the full potential of hBN semiconductors for high-efficiency neutron detectors, a relatively thick hBN film (i.e., ~80-µm-thick ^{10}B-enriched hBN layer) is required, and the detector geometry needs to be designed in such a way that charges are collected along the plane of hBN rather than perpendicular to the hBN plane. Here, we report on the epitaxial growth of hBN on *c*-plane sapphire substrates by cold wall chemical vapor deposition (CVD) with a growth rate >5 µm per hour, lift-off of a relatively thick (~15 µm) hBN film as a free-standing film, and transfer to another substrate. These free-standing films provide a unique opportunity to fabricate vertical as well as lateral metal–hBN–metal (MSM) device structures and determine the in-plane and out-of-plane transport properties of such films. Our study shows that even the bulk hBN film has a large anisotropy in electrical transport properties along the *a*- and *c*-planes. The mobility–carrier lifetime product ($\mu\tau$) of the CVD-grown free-standing film is a few orders of magnitude higher along the plane than along the out-of-plane direction. Furthermore, the in-plane $\mu\tau$ of such hBN grown by CVD at such a high growth rate and at a relatively low

© 2016 The Japan Society of Applied Physics

growth temperature (~1300 °C) is comparable to that of GaN. These results are very promising for fabricating very thick and large-area free-standing hBN films with reasonable optical and crystalline quality for many device applications.

hBN epitaxial layers were synthesized by cold wall CVD using a triethylboron (TEB) source and ammonia (NH_3) as B and N precursors, respectively. Prior to epilayer growth, a nitridation of sapphire at ~900 °C is first carried out by passing NH_3 for 10 min. This nitridation step is very critical for obtaining subsequently grown hBN films with good crystalline quality. After nitridation, the epitaxial growth of hBN starts and then the temperature is quickly ramped to ~1300 °C. The growth rate was varied from 0.5 to 5 µm per hour. If the thickness of hBN on sapphire is below 1 µm, the hBN film is relatively stable and does not lift off. However, if the thickness is more than 2 µm, the hBN film lifts off from the substrate. Such a thick film can be transferred to other substrates as a free-standing film or attached to other substrates using adhesive tape. If the film is >10 µm thick, the lifted hBN film is flexible and can easily be handled by tweezers and cleaved into pieces of a few centimeters on a side. The surface of the free-standing hBN film on the lifted-off side is very smooth and shiny; however, the grown side looks relatively rough. X-ray diffraction (XRD) was employed to determine the crystalline quality of the free-standing film placed onto another sapphire substrate. Absorption spectra were taken to determine the band edge absorption and Raman spectra were also taken to determine the optical quality of the film. The XRD θ–2θ scan of a 15-µm-thick free-standing hBN film transferred to another sapphire substrate is shown in Fig. 1(a). The hBN crystal orientation is along the c-axis as the hBN was grown on a c-plane sapphire substrate and transferred to another c-plane sapphire substrate for XRD. The reference (006) sapphire peak is at 2θ, which is equal to 41.7° in the XRD plot. The 2θ peak for hBN at about 26° corresponds to a c-lattice constant of ~6.8 Å, which is slightly higher than the bulk c-lattice constant of hBN (i.e., $c = 6.66$ Å[11]). The XRD rocking curve of the (002) reflection of the hBN film has a FWHM of 0.6° (not shown here). The FWHM indicates that the crystalline quality of CVD-grown hBN films is in an early developmental stage and can be improved further with optimized growth conditions. The possible route to improve the crystalline quality is to reduce the growth rate and increase the growth temperature further. Figure 1(b) shows the Raman spectra of a 15-µm-thick free-standing hBN film measured using a Witec Alpha 300R confocal Raman imaging system with 532 nm laser excitation. The mode $\Delta\sigma = 1369\,\text{cm}^{-1}$ corresponds to the E_{2g} symmetry vibration of hBN due to the in-plane stretching of B and N atoms, which is close to that of bulk hBN crystals ($\Delta\sigma = 1367\,\text{cm}^{-1}$).[11] The FWHM of the room-temperature Raman line is ~30 cm^{-1}, which is a few times higher than that of the bulk hBN (i.e., FWHM = 9 cm^{-1}) grown by flux methods using Ni and Cr solvent mixtures.[11] We repeated the Raman measurement at different points of the film and found similar values. Nevertheless, these results are reasonably good for CVD-grown films at such a high growth rate at a relatively low temperature. We also measured the absorption spectra of the hBN film using a UV–vis–NIR spectrometer from Varian (175 to 3300 nm). The absorption spectrum is shown in Fig. 2. The inset shows the optical microscopy image of a ~0.5-µm-thick film grown on a 2-in. sapphire substrate. A very strong absorption around 220 nm has been observed, which is attributed to the near-bandgap absorption of the hBN film.[12]

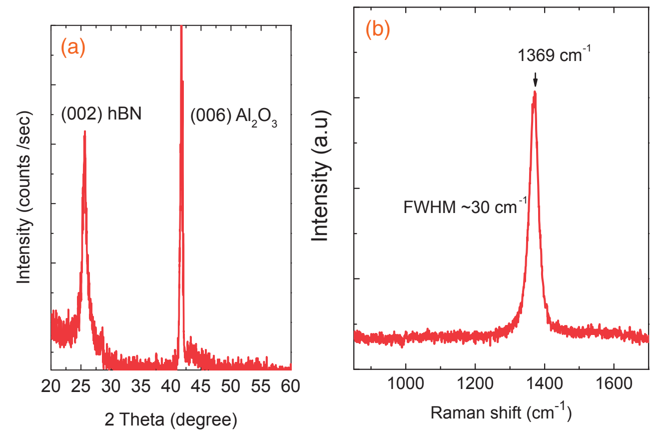

Fig. 1. (a) XRD θ–2θ scan of 15-µm-thick free-standing hBN film sitting on a sapphire substrate. (b) Raman spectra of the same film.

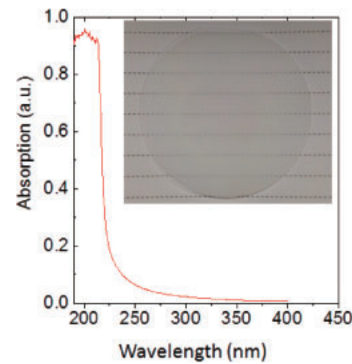

Fig. 2. Absorption spectra of about 0.5-µm-thick hBN film grown on a 2-in. c-plane sapphire substrate using the same growth condition of the 15-µm-thick hBN film. The inset shows the optical microscopy image of the hBN film grown on the 2-in. sapphire substrate. The hBN film can be transferred to another substrate with the use of adhesive wax or tape for bonding and the application of tangential force.

One of the potential applications of high-quality hBN could be the realization of large-area solid-state thermal neutron detectors with improved detection efficiency, owing to the high density of the boron atom in hBN. The full charge collection in a semiconducting detector material is determined by an important parameter, carrier mobility–lifetime product ($\mu\tau$), which strongly depends on the crystalline quality of the material. For a full charge collection, the $\mu\tau$ values for both carriers should be sufficiently large so $\mu\tau E$ with E being the electric field should be larger than the electrode spacing of the detector. In this work, MSM structures in lateral and vertical configurations were used to measure the $\mu\tau$ values for both carriers along the plane and out of plane in a free-standing hBN film grown by CVD. To fabricate a lateral MSM device, 300 nm SiO_2 was deposited on one side of the film, and the film was then cleaved into rectangular bars about 1 mm wide and several mm long. These hBN strips were fixed on a sapphire substrate by Kapton tapes and 200 nm Ni was deposited on both edges of the hBN strips with a shadow mask using an e-beam

© 2016 The Japan Society of Applied Physics

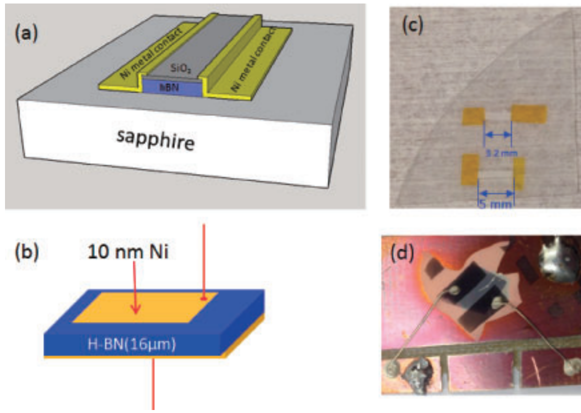

Fig. 3. (a) Schematic of a lateral-type MSM device, (b) that of a vertical-type MSM device, (c) optical image of 4- and 16-µm-thick freestanding hBN strips mounted on a sapphire substrate with Kapton tape prior to Ni metal deposition, and (d) optical image of vertical-type MSM device. The 300 nm SiO_2 deposited in lateral-type devices allows the collection of charge carriers only through the cleaved edges in contact with metal.

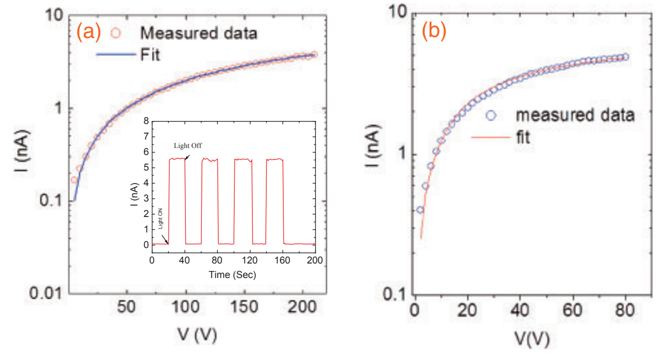

Fig. 4. (a) Photocurrent versus applied bias voltage under UV light exposure from mercury lamp (circles represent measured data); the line is the fitting using Eq. (1). For the lateral device, the extracted in-plane $\mu_e\tau_e$ and $\mu_h\tau_h$ for electrons and holes are $\sim 2.8 \times 10^{-5}$ and $\sim 4.85 \times 10^{-6}\,\mathrm{cm^2/V}$, respectively. (b) For the vertical device, the extracted out-of-plane $\mu_e\tau_e$ and $\mu_h\tau_h$ are $\sim 5.8 \times 10^{-8}$ and $\sim 6.1 \times 10^{-9}\,\mathrm{cm^2/V}$, respectively. The inset in (a) shows the effect of manual light source ON–OFF on photocurrent when the device is biased at 50 V. The very sharp fall and rise of photocurrent with light source OFF–ON indicates that there is no persistent photoconductivity in the hBN thin films.

evaporator. On the other hand, to fabricate a vertical MSM device, a 200 nm Ni layer was deposited on one side of a $5 \times 5\,\mathrm{mm^2}$ free-standing hBN film; the film was then mounted with silver paste to a sapphire substrate, followed by a 10 nm Ni layer deposited on the other side except the edges using a shadow mask. The schematic device structures and optical microscopy images are shown in Figs. 3(a)–3(d). To extract the $\mu\tau$ values for electrons and holes, photocurrent (I) as a function of applied bias was measured for both configurations under UV light excitation. Photocurrent as a function of voltage is given by Many's equation,[13,14)]

$$I(V) = I_0\left\{\frac{\mu_e\tau_e}{W^2}V\left[1 - \exp\left(\frac{\mu_e\tau_e}{W^2}V\right)^{-1}\right] + \frac{\mu_h\tau_h}{W^2}V\left[1 - \exp\left(\frac{\mu_h\tau_h}{W^2}V\right)^{-1}\right]\right\}, \quad (1)$$

where V is the applied bias, and W is the strip width for a lateral device or the thickness of the hBN film for a vertical device. The measured photocurrents as a function of bias voltage for both lateral and vertical MSM devices are shown in Figs. 4(a) and 4(b), respectively. The low value of the current indicates that the films are highly resistive as grown. The measured photocurrents are fitted using Eq. (1); the $\mu\tau$ values for electrons and holes for both lateral and vertical configurations are extracted. The inset in Fig. 4(a) shows the photocurrent response with the turn ON–OFF of the light source at a fixed bias voltage of 50 V. The very sharp rise and fall of the photocurrent with light ON–OFF indicates that there is no significant persistent photoconductivity in the hBN film. The extracted in-plane $\mu_e\tau_e$ and $\mu_h\tau_h$ for electrons and holes are $\sim 2.8 \times 10^{-5}$ and $\sim 4.85 \times 10^{-6}\,\mathrm{cm^2/V}$, measured from lateral carrier collection, whereas the out-of-plane $\mu_e\tau_e$ and $\mu_h\tau_h$ are $\sim 5.8 \times 10^{-8}$ and $\sim 6.1 \times 10^{-9}\,\mathrm{cm^2/V}$, measured from vertical carrier collection, respectively. The $\mu\tau$ product is a few orders of magnitude higher along the plane than along the out of plane. As hBN is a layered material like graphene, the charge carriers are expected to have a much higher mobility along the plane than along the out of plane. This experimental result demonstrates that charge carriers even in bulk hBN films [although the hBN film studied here is not a very high quality single crystal, as evidenced by XRD in Fig. 1(a)] demonstrate a 2D character, consistent with the 2D character of excitons in 3D bulk crystals as suggested in Ref. 10. The in-plane $\mu\tau$ values for electrons and holes are an order of magnitude higher than previously reported for hBN thin films grown by MOCVD, and comparable to that of GaN.[15)] In order to minimize the surface conduction (if any) of the hBN film for in-plane conductivity measurement, we deposited SiO_2 on the surfaces of the free-standing hBN film, and metal electrodes were deposited in cleaved facets in many samples; similar results were found. Thus, the experimentally observed significantly higher $\mu\tau$ values in our free-standing hBN film suggest that hBN could be an ideal candidate for detector materials if the device is designed in such a way that carriers move along the plane to reach the respective electrode before they recombine. These anisotropic carrier transports observed in the hBN film demonstrate that hBN is also an ideal candidate for studying 2D transport properties even in bulk film and offers numerous opportunities for designing highly efficient electronic and optoelectronic devices.

In determining $\mu\tau$ values, we have used UV light (mercury light) for carrier excitation. In this case, the photon intensity is generally high and the carriers generated could saturate some of the defects and traps present in the crystal so that $\mu\tau$ could be overestimated. To avoid this, lateral-configuration MSM strip detectors of 2 mm width and 1 cm length were fabricated using a 4-µm-thick free-standing hBN film. The neutron count rate above noise level was measured as a function of applied voltage under thermal neutron exposure from a ^{256}Cf moderated source, where the excitation flux is much lower than the UV light excitation. In this case, the current (I) in Eq. (1) is simply replaced by the count rate (C) and Eq. (1) now becomes

$$C(V) = C_0\left\{\frac{\mu_e\tau_e}{W^2}V\left[1 - \exp\left(\frac{\mu_e\tau_e}{W^2}V\right)^{-1}\right] + \frac{\mu_h\tau_h}{W^2}V\left[1 - \exp\left(\frac{\mu_h\tau_h}{W^2}V\right)^{-1}\right]\right\}. \quad (2)$$

© 2016 The Japan Society of Applied Physics

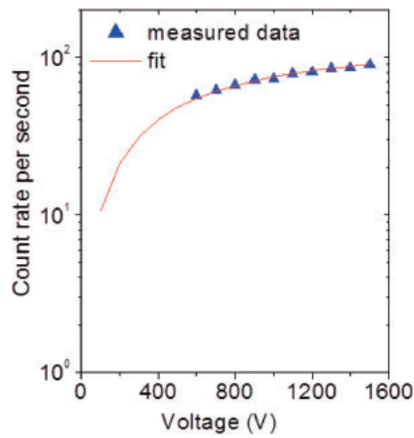

Fig. 5. Count rate (count rate recorder above the lower level discrimination) vs bias voltage for lateral-type MSM device for 4-μm-thick hBN film under thermal neutron incident from a moderated ^{252}Cf source (circles are measured data) and fitting of the measured data using Eq. (2) (solid line). The $\mu_e\tau_e$ and $\mu_h\tau_h$ values extracted are $\sim 3.6 \times 10^{-5}$ and $\sim 3.2 \times 10^{-6}$ cm^2/V, respectively. These values are similar to those measured under UV light exposure.

The measured count rate as a function of applied bias and the fitting of measured data with Eq. (2) are shown in Fig. 5. The extracted $\mu_e\tau_e$ and $\mu_h\tau_h$ for electrons and holes under thermal neutron excitation are $\sim 3.6 \times 10^{-5}$ and $\sim 3.2 \times 10^{-6}$ cm^2/V, respectively, measured from lateral carrier configuration. These $\mu_e\tau_e$ and $\mu_h\tau_h$ values measured under thermal neutron excitation are close to those measured under UV light excitation.

In summary, we have grown hBN films up to 15 μm thick with a growth rate of 5 μm per hour in a CVD system and studied the structural, optical, and transport properties of free-standing hBN films. The free-standing films allow the fabrication of metal–hBN–metal structures in lateral and vertical configurations. From these vertical and lateral device structures, the in-plane and out-of-plane mobility–lifetime products ($\mu\tau$) of electrons and holes in free-standing hBN films were extracted from current–voltage (I–V) characteristics under UV light exposure and count rate–voltage characteristics under thermal neutron exposure. The extracted in-plane $\mu_e\tau_e$ and $\mu_h\tau_h$ for electrons and holes are $\sim 2.8 \times 10^{-5}$ and $\sim 4.85 \times 10^{-6}$ cm^2/V, whereas the out-of-plane $\mu_e\tau_e$ and $\mu_h\tau_h$ are $\sim 5.8 \times 10^{-8}$ and $\sim 6.1 \times 10^{-9}$ cm^2/V, respectively. The $\mu\tau$ product along the plane is a few orders of magnitude higher than that along the out of plane. These anisotropic carrier transports observed in hBN thin films demonstrate that hBN is an ideal candidate for studying the 2D character of charge carriers in a 3D system. These results offer a great opportunity to design highly efficient electronic and optoelectronic devices and solid-state thermal neutron detectors for many applications.

Acknowledgments This work has been supported by the US Department of Homeland Security, Domestic Nuclear Detection Office, under competitively awarded grants ECCS-1348269 and 2013-DN-077-ER001. This support does not constitute an express or implied endorsement on the part of the Government.

1) R. Haubner, M. Wilhelm, R. Weissenbacher, and B. Lux, in *High Performance Non-Oxide Ceramics II*, ed. M. Jansen (Springer, Heidelberg, 2002) Structure and Bonding, Vol. 102, Chap. 1, p. 1.
2) Y. Kubota, K. Watanabe, O. Tsuda, and T. Taniguchi, Science **317**, 932 (2007).
3) T. Sugino, C. Kimura, and T. Yamamoto, Appl. Phys. Lett. **80**, 3602 (2002).
4) K. Watanabe, T. Taniguchi, T. Niiyama, K. Miya, and M. Taniguchi, Nat. Photonics **3**, 591 (2009).
5) D. Pacilé, J. C. Meyer, Ç. Ö. Girit, and A. Zettl, Appl. Phys. Lett. **92**, 133107 (2008).
6) L. Song, L. Ci, H. Lu, P. B. Sorokin, C. Jin, J. Ni, A. G. Kvashnin, D. G. Kvashnin, J. Lou, B. I. Yakobson, and P. M. Ajayan, Nano Lett. **10**, 3209 (2010).
7) S. Dai, Z. Fei, Q. Ma, A. S. Rodin, M. Wagner, A. S. McLeod, M. K. Liu, W. Gannett, W. Regan, K. Watanabe, T. Taniguchi, M. Thiemens, G. Dominguez, A. H. Castro Neto, A. Zettl, F. Keilmann, P. Jarillo-Herrero, M. M. Fogler, and D. N. Basov, Science **343**, 1125 (2014).
8) R. Dahal, K. C. Huang, N. LiCausi, J. Q. Lu, I. Bhat, J. Clinton, and Y. Danon, Appl. Phys. Lett. **101**, 171112 (2012).
9) J. Li, S. Majety, R. Dahal, W. P. Zhao, J. Y. Lin, and H. X. Jiang, Appl. Phys. Lett. **101**, 171112 (2012).
10) J. Li, R. Dahal, S. Majety, J. Y. Lin, and H. X. Jiang, Nucl. Instrum. Methods Phys. Res., Sect. A **654**, 417 (2011).
11) X. K. Cao, B. Clubine, J. H. Edgar, J. Y. Lin, and H. X. Jiang, Appl. Phys. Lett. **103**, 191106 (2013).
12) R. Dahal, J. Li, S. Majety, B. N. Pantha, X. K. Cao, J. Y. Lin, and H. X. Jiang, Appl. Phys. Lett. **98**, 211110 (2011).
13) A. Many, J. Phys. Chem. Solids **26**, 575 (1965).
14) Y. Nemirovsky, A. Ruzin, G. Asa, and J. Gorelik, J. Electron. Mater. **25**, 1221 (1996).
15) P. Parkinson, C. Dodson, H. J. Joyce, K. A. Bertness, N. A. Sanford, L. M. Herz, and M. B. Johnston, Nano Lett. **12**, 4600 (2012).

© 2016 The Japan Society of Applied Physics